2016

Virus–host interactions: insights from the replication cycle of the large *Paramecium bursaria* chlorella virus

Elad Milrot

Yael Mutsafi

Yael Fridmann-Sirkis

Eyal Shimoni

Katya Rechav

See next page for additional authors

Authors
Elad Milrot, Yael Mutsafi, Yael Fridmann-Sirkis, Eyal Shimoni, Katya Rechav, James Gurnon, James L. Van Etten, and Abraham Minsky

Cellular Microbiology (2016) **18**(1), 3–16

doi:10.1111/cmi.12486
First published online 27 August 2015

Virus–host interactions: insights from the replication cycle of the large *Paramecium bursaria chlorella virus*

Elad Milrot,[1]* Yael Mutsafi,[1] Yael Fridmann-Sirkis,[1] Eyal Shimoni,[2] Katya Rechav,[2] James R. Gurnon,[3] James L. Van Etten[3] and Abraham Minsky[1]*

[1]*Department of Structural Biology, Weizmann Institute of Science, Rehovot 76100, Israel.*

[2]*Department of Chemical Research Support, Weizmann Institute of Science, Rehovot 76100, Israel.*

[3]*Department of Plant Pathology and Nebraska Center for Virology, University of Nebraska, Lincoln, NE, 68583-0900, USA.*

Summary

The increasing interest in cytoplasmic factories generated by eukaryotic-infecting viruses stems from the realization that these highly ordered assemblies may contribute fundamental novel insights to the functional significance of order in cellular biology. Here, we report the formation process and structural features of the cytoplasmic factories of the large dsDNA virus *Paramecium bursaria chlorella* virus 1 (PBCV-1). By combining diverse imaging techniques, including scanning transmission electron microscopy tomography and focused ion beam technologies, we show that the architecture and mode of formation of PBCV-1 factories are significantly different from those generated by their evolutionary relatives Vaccinia and *Mimivirus*. Specifically, PBCV-1 factories consist of a network of single membrane bilayers acting as capsid templates in the central region, and viral genomes spread throughout the host cytoplasm but excluded from the membrane-containing sites. In sharp contrast, factories generated by *Mimivirus* have viral genomes in their core, with membrane biogenesis region located at their periphery. Yet, all viral factories appear to share structural features that are essential for their function. In addition, our studies support the notion that PBCV-1 infection, which was recently reported to result in significant pathological outcomes in humans and mice, proceeds through a bacteriophage -like infection pathway.

Received 16 June, 2015; revised 9 July, 2015; accepted 15 July, 2015. *For correspondence. E-mail elad.milrot@weizmann.ac.il; avi.minsky@weizmann.ac.il; Tel. (+972) 89342003; Fax (+972) 89344149.

Introduction

An exciting development in cellular and physical biology is the realization that organelles previously thought to be randomly organized are in fact highly ordered and that this order critically affects the functions of these organelles (Takizawa *et al*., 2008; Thanbichler and Shapiro, 2008). Specifically, the advent of imaging and biochemical methodologies revealed that chromosomes occupy well-defined territories within eukaryotic nuclei (Meaburn and Misteli, 2007; Misteli, 2007), and that this particular positioning has profound functional implications on fundamental genomic transactions (Misteli, 2004; Takizawa *et al*., 2008; Edelman and Fraser, 2012). Equally interesting is the recent realization that bacterial cells localize nucleic acids and proteins to specific cellular locations and that such well-defined organization is vital for regulatory processes (Gitai, 2005; Thanbichler and Shapiro, 2008; Shapiro *et al*., 2009; Llopis *et al*., 2010; Bowman *et al*., 2011; Nevo-Dinur *et al*., 2011). Another example of the generation of intracellular organelles characterized by distinct compartmentalization that is apparently essential for their function is provided by viral replication centres. Such specialized sites were initially detected during the infection of positive-strand RNA ((+)RNA) viruses. Infection by these viruses involves massive reorganization of the host cytoskeleton and membrane networks, leading to the formation of a platform coined the viral factory (VF), in which genome replication and virion assembly are effectively coordinated (Ahlquist, 2006; Fontana *et al*., 2007; Kopek *et al*., 2007; den Boon and Ahlquist, 2010; den Boon *et al*., 2010; Hsu *et al*., 2010; Netherton and Wileman, 2011; de Castro *et al*., 2013).

Novel insights into the generation, structure and function of VFs are provided by studies on the infection cycles of nucleocytoplasmic large DNA viruses (NCLDVs), which include the eukaryotic-infecting families Poxviridae, Asfarviridae, Iridoviridae, Phycodnaviridae, Mimiviridae and Marseillevirdae. All members of this clade are characterized by a large size as well as by the ordered and elaborate viral factories they generate in the

PMID: 26248343
https://www.ncbi.nlm.nih.gov/pubmed/26248343

cytoplasm of their hosts (Novoa *et al*., 2005; Wileman, 2006; Netherton and Wileman, 2011; de Castro *et al*., 2013; Mutsafi *et al*., 2014). In particular, studies conducted on Vaccinia virus (Mallardo *et al*., 2001; Condit, 2007; Katsafanas and Moss, 2007; Miller and Krijnse-Locker, 2008; Chlanda *et al*., 2009; Suárez *et al*., 2013; Moss, 2015), as well as on the Mimivirus (Raoult *et al*., 2004; Zauberman *et al*., 2008; Mutsafi *et al*., 2010; Mutsafi *et al*., 2013; Suárez *et al*., 2013), highlight the complexity, long-range order and compartmentalization of functions in viral factories.

These observations imply that, as is the case in nuclei, bacteria and viral factories of (+)RNA viruses, precise compartmentalization of functions is an intrinsic trait of cytoplasmic factories generated by large dsDNA viruses, thus implying a functional similarity between nuclei, bacteria and viral factories (Miller and Krijnse-Locker, 2008). Indeed, it has been proposed that viral factories should be considered as 'mini-nuclei' (Tolonen *et al*., 2001) that might have played an important role in the evolution of eukaryotic nuclei (Bell, 2006). It was also suggested that VFs can be viewed as the actual living stage of viruses (Claverie *et al*., 2009; Claverie and Abergel, 2010). This conjecture is further supported by the observation that membranes play a central role in the assembly of viruses (Tolonen *et al*., 2001; Kopek *et al*., 2007; Miller and Krijnse-Locker, 2008; den Boon and Ahlquist, 2010; Laliberte and Moss, 2010; Mutsafi *et al*., 2013; Suárez *et al*., 2013; Suárez *et al*., 2015), as is the case in eukaryotic nuclei.

Prompted by these considerations, as well as by studies demonstrating that VFs produced by Vaccinia virus and *Mimivirus* reveal substantial resemblance (Krijnse-Locker et al., 2013; Mutsafi *et al*., 2010; Suárez *et al*., 2013) but also significant differences (Katsafanas and Moss, 2007; Mutsafi *et al*., 2013; Mutsafi *et al*., 2014), we investigated the cytoplasmic factories generated by the dsDNA-containing *Paramecium bursaria chlorella virus* (PBCV-1). PBCV-1, which is a member of the Phycodnaviridae family that belongs to the NCLDV clade (Iyer *et al*., 2001), is a large (~190 nm in diameter), dsDNA (331 kbp) icosahedral virus that replicates in unicellular green algae (Meints *et al*., 1986; Van Etten, 2003; Yamada *et al*., 2006; Van Etten *et al*., 2010; Van Etten and Dunigan, 2012). The infection cycle consists of a phage-like genome ejection into the host cytoplasm followed by its presumed translocation to the nucleus where early transcription, followed by replication occurs. Newly synthesized genomes are assumed to be released into the cytoplasm where viral factories are generated (Van Etten, 2003).

Paramecium bursaria chlorella virus 1 and related Phycodnaviruses recently attracted interest following studies indicating that the largest currently known viruses, *Pandoraviruses* (Philippe *et al*., 2013), are evolutionary related to Phycodnaviruses (Yutin and Koonin, 2013). In a separate study, DNA sequences of the Phycodnavirus *Acanthocystis turfacea chlorella virus* 1 (ATCV-1) were detected in human throat swabs and their presence was associated with a statistically significant decrease in cognitive behaviour (Yolken *et al*., 2014). Furthermore, mice fed with ATCV-1-infected algae exhibited performance decreases in cognitive tests (Yolken *et al*., 2014).

To investigate viral factories generated by PBCV-1, we used a wide array of imaging techniques including fluorescence microscopy, immunolabelling, electron microscopy of cryo-preserved specimens, as well as novel scanning-transmission electron microscopy (STEM) tomography and focused ion beam (FIB) microscopy. Our observations reveal that, as is the case in factories of (+)RNA viruses, Vaccinia and *Mimivirus*, membranes play a central role in the assembly of PBCV-1 factories. Yet, in contrast to Vaccinia and *Mimivirus* factories, in which the inner core consists of replicated and transcribed genomes with membrane synthesis and capsid assembly occurring at the periphery (Mallardo *et al*., 2002; Mutsafi *et al*., 2013; Suárez *et al*., 2013; Mutsafi *et al*., 2014), PBCV-1 factories consist of a central membrane and capsid region with viral genomes localized at the periphery. Viral factories thus represent an intriguing example of efficient intracellular self-assembly processes that might provide new insights into factors that shaped structure-function correlations in nuclei and bacteria as well as into the mechanisms responsible for cellular organization in general.

Results

Chlorovirus PBCV-1 infection of *Chlorella variabilis* is initiated by the ejection of its dsDNA genome into the host cytoplasm in a phage-like process (Van Etten and Dunigan, 2012), which is followed by its presumed translocation into the nucleus. Early PBCV-1 transcription was detected within 7 min post infection (PI) (Blanc *et al*., 2014), followed by viral DNA synthesis at 60 min PI (Van Etten *et al*., 1984). The studies reported here focus on the cytoplasmic factories generated by PBCV-1 shortly after the release of its replicated genomes from the host nuclei into the cytoplasm.

Initial structural alterations following Paramecium bursaria chlorella virus *1 infection are nuclei deformations*

High-resolution electron microscopy of cryo-immobilized PBCV-1 *C. variabilis*-infected cells as well as fluorescence imaging in which the fluorescent probes SYTO82 for DNA detection and $DiOC_6$, a specific membrane probe (Terasaki and Reese, 1992), were used to unravel

advanced stages of PBCV-1 infection. The first structural evidence of infection is observed already at 1 h PI, when deformed morphologies of host nuclei were detected, as previously reported (Meints *et al*., 1986). Specifically, nuclei of infected cells lose their spherical shape that characterizes non-infected cells (Fig. 1A and C) and assume elongated or crescent-like morphologies that reveal enhanced heterochromicity (areas near the nuclear membrane that are heavily stained for DNA) (Fig. 1B, D and E). It is tempting to propose that such modified nuclear structures reflect extensive degradation of host DNA that begins shortly after PBCV-1 infection (Agarkova *et al*., 2006), as well as viral DNA replication, previously shown to occur at 60 min PI (Meints *et al*., 1986; Van Etten *et al*., 1984; Van Etten, 2003; Yamada *et al*., 2006). Notably, similar alterations in nuclear morphology were observed following the infection of *Acanthamoeba* cells by the giant *Pandoravirus* (Philippe *et al*., 2013).

Host membranes play a central role in the assembly and structure of Paramecium bursaria chlorella virus *1 cytoplasmic factories*

At 2 h PI, viral factories are detected in the host cytoplasm. In order to characterize the spatial organization of these assembly sites, we used STEM tomography that provides detailed 3-dimensional structural data of thick (> 300 nm) specimens (Aoyama *et al*., 2008). Sequential tomography slices of early VFs reveal rosette-like crescent structures (Fig. 2A–D) that are particularly evident in the slice shown in panel C. The crescent structures consist of two distinct layers characterized by different densities: an external angular capsid shell indicated by yellow arrowheads and yellow structures and an internal membrane bilayer shown in light blue.

As is the case in *Mimivirus* factories (Mutsafi *et al*., 2013; Suárez *et al*., 2013; Mutsafi *et al*., 2014), the angular structures consistently point away from the central region of PBCV-1 factories from which host ribosomes and other organelles are excluded. Such exclusion is presumably effected by massive accumulation of viral products mainly consisting of membrane bilayer sheets (further discussed in the succeeding paragraphs), required for a continuous assembly of new progeny virions. Light blue arrowheads in the tomographic slices (Fig. 2A–D), as well as in 3-dimensional surface rendering representation derived from STEM tomography (Fig. 2E and F) point to open single membrane sheets that act as templates for angular capsids (yellow arrowheads). Notably, a role of membrane bilayers in capsid scaffolding has been demonstrated for Vaccinia virus (Risco *et al*., 2002; Szajner *et al*., 2005; Miller and Krijnse-Locker, 2008; Chichon *et al*., 2009; Chlanda *et al*., 2009) and *Mimivirus* (Krijnse-Locker *et al*., 2013; Mutsafi *et al*., 2013; Mutsafi *et al*., 2014; Suárez *et al*., 2013). A 3D surface rendering of the rosette-like PBCV-1 crescent structures derived from STEM tomography is shown in Movie S1.

Further, STEM analyses of 2–3 h PI PBCV-1 infected cells reveal that factory generation is accompanied by massive accumulation of membrane cisternae (blue arrowheads in Fig. 3) that partially surround the VFs (Fig. 3C, D, G and H) and in some cases deeply

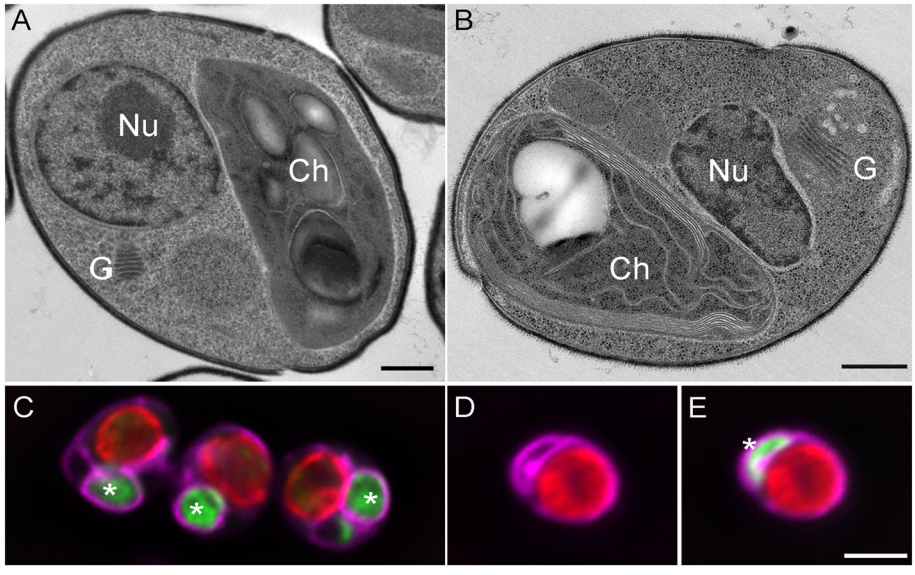

Fig. 1. PBCV-1-induced alteration of host nuclear morphology.
A, B. *C. variabilis* cells were subjected to HPF-FS and analysed by TEM. (A) Control (mock-infected) cell shows a spherical nuclear morphology. (B) 1 h PI cell exhibiting a characteristically deformed nuclear morphology. Nu: Nucleus, Ch: Chloroplast, G: Golgi.
C–E. Representative 0.2 μm slices of de-convoluted fluorescence images showing non-infected (C) and 1 h PI infected cell (D, E) stained for DNA (SYTO82, green), membranes ($DiOC_6$, magenta) and chloroplast auto-florescence (red). (C) Non-infected cells exhibiting round nuclear morphology. (D) Cellular and nuclear contours determined by membrane $DiOC_6$ staining (magenta) and chlorophyll (red). The highly aberrant nuclear structure is evident. (E) Overlay image of DNA, membranes and chloroplast. Asterisks mark host nuclei. Scale bars: A, B: 500 nm, C–E: 2 μm.

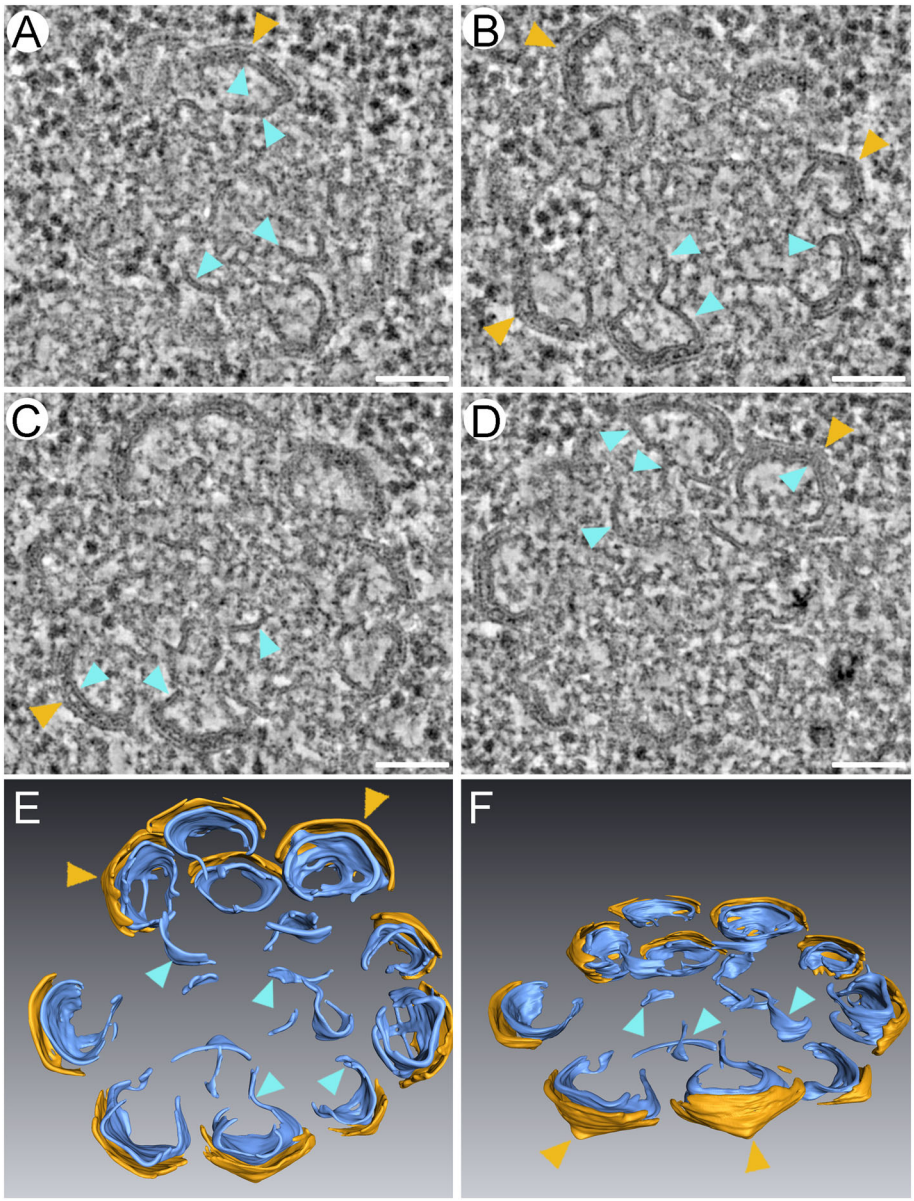

Fig. 2. Rosette-like architecture of early PBCV-1 factories (Movie S1).
A–D. Four successive 10 nm thick slices from a STEM tomogram showing a rosette-like cytoplasmic factory of PBCV-1 in a 2 h PI *C. variabilis* cell. Light blue arrowheads point to open sheets single membrane bilayers that accumulate in the centre of PBCV-1 factories and yellow arrowheads indicate capsids generated at the outer sites of the membrane bilayers.
E, **F**. Surface rendering of the tomogram showing top (E) and edge (F) views of a PBCV-1 factory. Open membrane sheets and capsids are depicted in light blue and yellow respectively. Scale bars: 100 nm.

penetrate the factory cores (red arrow in panel 3G). Cisternae appear to bud out from rough endoplasmic reticulum (ER) membranes as implied by multiple ribosomes decorating these structures (Fig. 3B, F). Tomography slices reveal that the cisternae are derived mainly from outer membranes of host nuclei, a finding consistent with previous observations on the source of Vaccinia membranes (Husain *et al.*, 2006). Notably, in contrast to open single-bilayer membrane sheets present in the centre of the VFs (Figs 2 and 3; light blue arrowheads), host cisternae detected at the periphery of the VFs are composed of double bilayers as determined by their width (Fig. 3; blue arrowheads). As discussed in the succeeding paragraphs, host ribosomes and presumably other host protein complexes are stripped away from the cisternae as they are translocated into the inner core of the PBCV-1 VFs and rendered into open single-bilayer sheets (light blue arrowheads in Figs 2 and 3D, G). The structures shown in Fig. 3C and D support the observations presented in Fig. 2, in that open membrane sheets generated within the VF cores (light blue) act as templates for the formation of capsid structures (yellow structures and arrowheads). Indeed, 3D surface rendering representation of the entire tomography volume (Fig. 3D) shows viral particles at three successive stages of capsid formation. Additional details on the accumulation of host membrane cisternae are

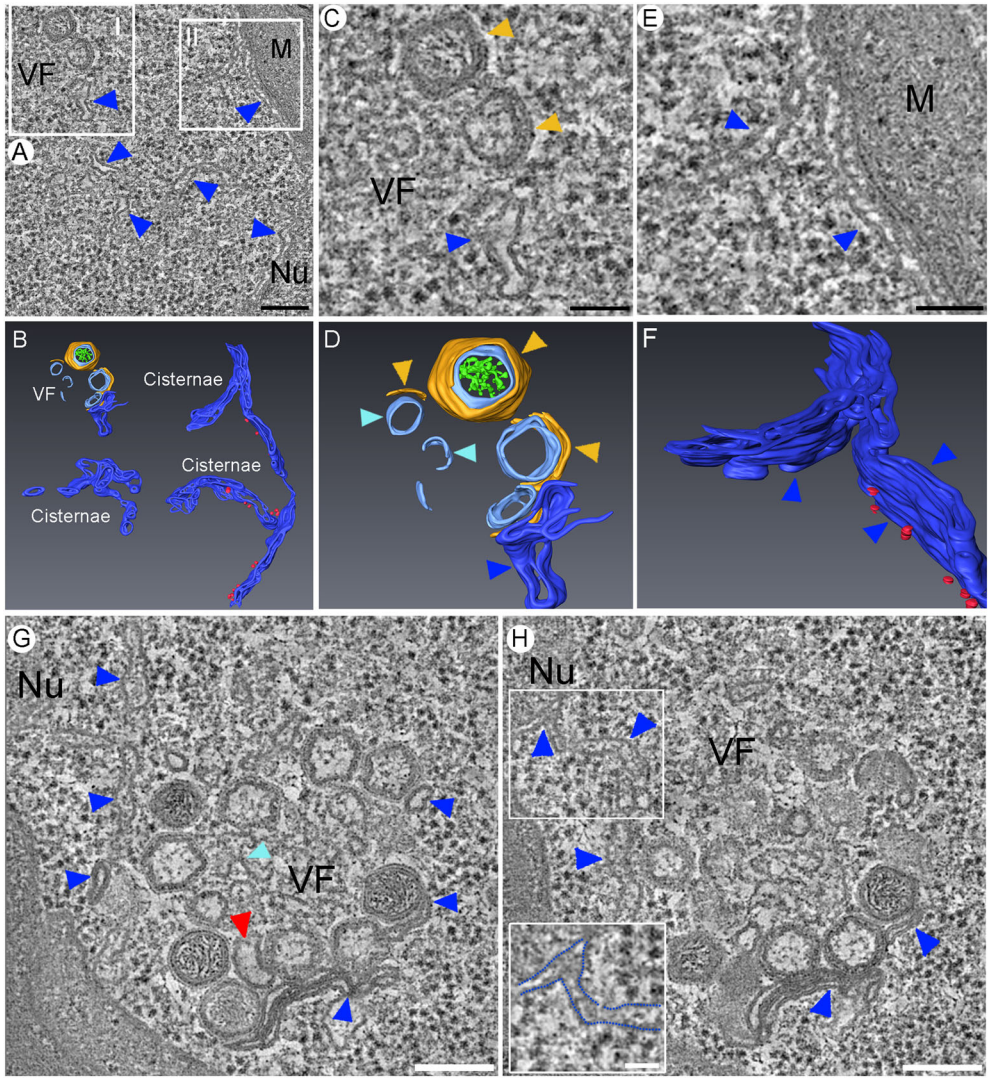

Fig. 3. PBCV-1 factories exhibit a complex membrane network composed of host cisternae and open membrane sheets (Figs S1, S2, Movies S2–S4).
A. 10 nm thick slice from a 250 nm thick STEM tomogram showing host cisternae (blue arrowheads) that accumulate at the periphery of the PBCV-1 factory in a 2 h PI *C. variabilis* cell. Nu: nucleus; M: mitochondria, VF: viral factory.
B. Surface segmentation of the tomogram shown in A, revealing host cisternae accumulating in the cytoplasm adjacent to the VF. Red spheres indicate ribosomes, implying that viral membranes derive from host rough ER.
C, **E**. Magnified images of regions I and II respectively, delineated in A. Blue arrowheads point to host cisternae localized at the periphery of VFs and yellow arrowheads indicate newly assembled capsids.
D, **F**. 3D surface rendering of tomogram slices C and E respectively, showing capsids at progressive assembly stages (D, yellow structures and arrowheads) generated at the surface of membrane sheets (light blue structures), as well as ribosome-decorated (red spheres) cisternae at the periphery of the VFs (F, blue structures and arrowheads).
G, **H**. Two 10 nm STEM tomography slices from a different 3 h PI cell, showing a PBCV-1 VF with newly assembled virions at various stages of maturation. Cisternae (blue arrowheads) partially enclose the viral assembly zone and occasionally penetrate deep into the factory (red arrowhead). The same tomogram shows cisternae budding from the outer nuclear membrane (upper inset marked with blue arrowheads). Lower inset shows an enlarged view of the upper inset, where cisternae are delineated with blue dots. Scale bars: A, G, H: 200 nm; C, E: 100 nm; inset in panel H: 50 nm.

provided in Figs S1 and S2, as well as in Movies S2–S4 that are derived from STEM tomography studies.

In contrast to Mimivirus and Vaccinia viral factories, cores of Paramecium bursaria chlorella virus *1 factories consist of membrane structures surrounded by viral genomes*

Contrast of membrane structures deteriorates in thick cryo-immobilized specimens used in STEM tomography, presumably due to limited infiltration of staining materials. However, in a recent study on stacked ER sheets, a method for overcoming this inherent drawback was described, using multiple ultra-thin sections of chemically preserved samples (Terasaki *et al.*, 2013). The results depicted in Figs 2 and 3 concerning the generation of the VFs of PBCV-1 were accordingly acquired with chemical fixation methods (see Experimental procedures). To further sub-

stantiate these observations, we used high-pressure-freezing followed by freeze substitution (HPF-FS) methodology, as well as fluorescence studies aimed at detecting both membrane structures and viral DNA.

Figure 4A–D and Fig. S3 show cryo-immobilized PBCV-1 infected chlorella cells at 3 and 4 h PI respectively. Cells reveal VFs with viral particles at various maturation stages, starting from crescent-shaped structures (light blue arrowheads pointing to single bilayer open membrane sheets and yellow arrowheads indicating capsids), partially assembled particles lacking DNA (red arrowhead) and mature virions (magenta arrowhead). Mature virions appear to be forced away from the VF core, presumably by the progressive and continuous generation of new progeny viral particles. Notably, open membrane sheets are clearly detected in VF centres (Fig. 4C and D; light blue arrowheads), thus corroborating observations derived from chemically preserved cells.

Figure 4E–G depicts a 3 h PI cell stained with SYTO82 (DNA staining, green) and $DiOC_6$ (membrane staining, magenta). The results presented in panel E indicate that at this PI time, the cytoplasm of infected cells is completely occupied by viral DNA, with punctuate patterns that most probably represent mature, DNA-containing viruses. Significantly, DNA is excluded from distinct regions in the cytoplasm (unstained 'holes' in panel E), which specifically correspond to membrane assembly zones, as determined by the $DiOC_6$ membrane staining as well as by an overlay of SYTO82 and $DiOC_6$ (Fig. 4F and G respectively). The spatial separation of DNA and membrane zones, with DNA present at the VF periphery and throughout the host cytoplasm, whereas membranes are localized at the centre of VFs, is indicated by an intensity plot profile of SYTO82 and $DiOC_6$ (Fig. 4H). Such a spatial separation is further confirmed by a Pearson correlation analysis, which is a measure of the degree of overlap of images recorded in different channels and thus indicative of colocalization or de-colocalization of specific substances (Adler *et al*., 2008). This analysis reveals a negative correlation between DNA and membrane intensity values (Fig. 4I). In addition, our fluorescence microscopy studies show that already at this relatively early infection stage, host nuclei are almost completely devoid of DNA (Fig. 4E–G, indicated with asterisks), in agreement with previous studies implying that host DNA is degraded by viral endonucleases shortly after infection (Agarkova *et al*., 2006; Yamada *et al*., 2006).

Viral factories generated by *Mimivirus* (Mutsafi *et al*., 2013; Mutsafi *et al*., 2014) and Vaccinia virus (Condit, 2007; Katsafanas and Moss, 2007; Miller and Krijnse-Locker, 2008; Chichon *et al*., 2009; Chlanda *et al*., 2009; Maruri-Avidal *et al*., 2013; Suárez *et al*., 2013; Moss, 2015) consist of an internal DNA core where viral DNA replication occurs and a peripheral domain in which membrane biosynthesis takes place. In sharp contrast, VFs produced by PBCV-1 are composed of a central membrane region surrounded by viral DNA (Figs 2–4). To support this observation, we conducted experiments aimed to localize DNA molecules using anti-DNA antibodies in thin (~70 nm) sections of cryo-immobilized infected chlorella cells at 2 h PI. The results reveal massive DNA egress from the host nucleus (Fig. 5A and B; note in particular the density extending from the nucleus towards the cytoplasm indicated by arrowheads in panel B). Panels C–F, depicting DNA localization in three additional PBCV-1 cryo-immobilized infected cells further support the notion that the cores of PBCV-1 VFs are depleted of DNA.

Insights into the pathway of genome encapsidation into pre-assembled capsids are provided in Fig. 6. Cryo-preserved PBCV-1-infected *C. variabilis* cells reveal that both internal membrane and capsid (light blue and yellow arrowheads, respectively) remain incomplete, thus forming a large aperture that enables efficient DNA packaging, as was shown to be the case for *Mimivirus* (Zauberman *et al*., 2008; Mutsafi *et al*., 2013). Encapsidated viral DNA is indicated with green arrowheads in Fig. 6C and D.

Focused ion beam-scanning electron microscopy studies of whole chlorella cells infected with *Paramecium bursaria chlorella virus* 1

To further analyse the PBCV-1 infection cycle, we used the novel FIB-SEM methodology that is widely used for material sciences studies but scarcely for biological research. In this method, a scanning electron beam is used to image the surface of cells or tissues that are progressively abraded by a focused ion beam that removes a thin layer of material (typically ~10 nm) from the surface. Electron microscopy of surfaces collected as the specimen is consumed by a focused ion beam are combined to generate ultrastructural 3D representation of the specimen (Bushby *et al*., 2011; Earl *et al*., 2013; Risco *et al*., 2014).

Our FIB-SEM results show a 3 h PI chlorella-infected cell exhibiting membrane cisternae extending from the host nucleus (Fig. 7A) and their disassembly at the VF periphery (blue arrowheads in Fig. 7B and C; Fig. S4; Movies S5 and S6). Segmentation of the volume derived from the FIB-SEM analysis is shown in Fig. 7D–E. Host nuclei (transparent blue) reveal elongated morphology, in agreement with our HPF-FS TEM and fluorescence studies (Fig. 1), and in sharp contrast with nuclei morphology of non-infected cells. We identified additional cisternae budding from different sites of the nucleus (blue arrowheads in Fig. 7E). FIB-SEM analysis of non-infected

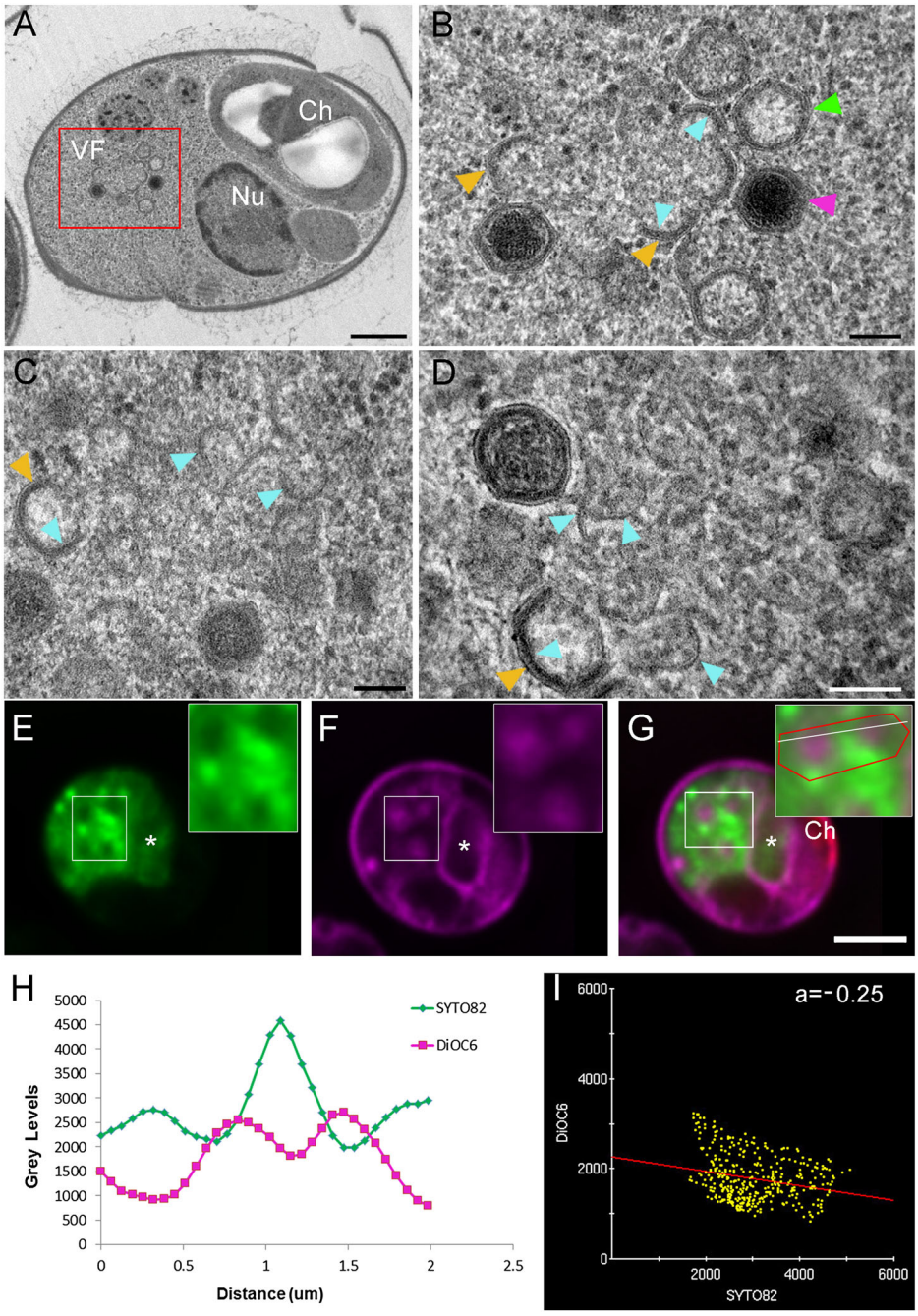

Fig. 4. TEM studies of a cryo-immobilized infected *C. variabilis* cell and fluorescence analyses of PBCV-1 VFs (corresponding to Fig. S3).
A. Low magnification view of a 3 h PI cryo-immobilized PBCV-1 infected *C. variabilis* cell.
B. High magnification view of the VF delineated in a red box in A.
C, **D**. High magnification views of VFs revealed by two different PBCV-1 infected cells studied by HPF-FS. Light blue arrowheads in B, C and D point to single bilayer membranes that act as templates for the generation of viral capsids (yellow arrowheads). Red and magenta arrowheads indicate pre-assembled empty and DNA containing virions respectively. These results, obtained by HPF-FS, reveal the presence of open single bilayer membranes and capsids at progressive assembly stages.
E–I. Fluorescence analyses of PBCV-1 VFs. (E-G) 0.2 μm slices of de-convoluted images showing a 3 h PI cell stained for DNA (E; SYTO82; green), membranes (F; $DiOC_6$; magenta) and overlay (G). 3 h PI cell stained for DNA (green) and membranes (magenta). (E) Cytoplasm is filled with DNA. Inset represents high magnification of the delineated area. (F) Viral membrane assembly zones located in the host cytoplasm. Inset shows high magnification of delineated area. (G) Overlay image showing viral DNA present throughout the cytoplasm but absent in regions of membrane accumulation at the centre of the VFs. White line and red contour (inset) were used for density plot profile and Pearson correlation respectively. (H) Density plot profile (distance values through the white line in the inset in G, from left to right), showing inverse correlation between DNA and membrane intensity values. DNA and membranes are indicated by green and magenta lines respectively. (I) Pearson correlation highlighting a negative correlation between DNA and membrane within the factory. Asterisks denote host nuclei. Scale bars: A: 500 nm; B–D: 100 nm; E–G: 2 μm.

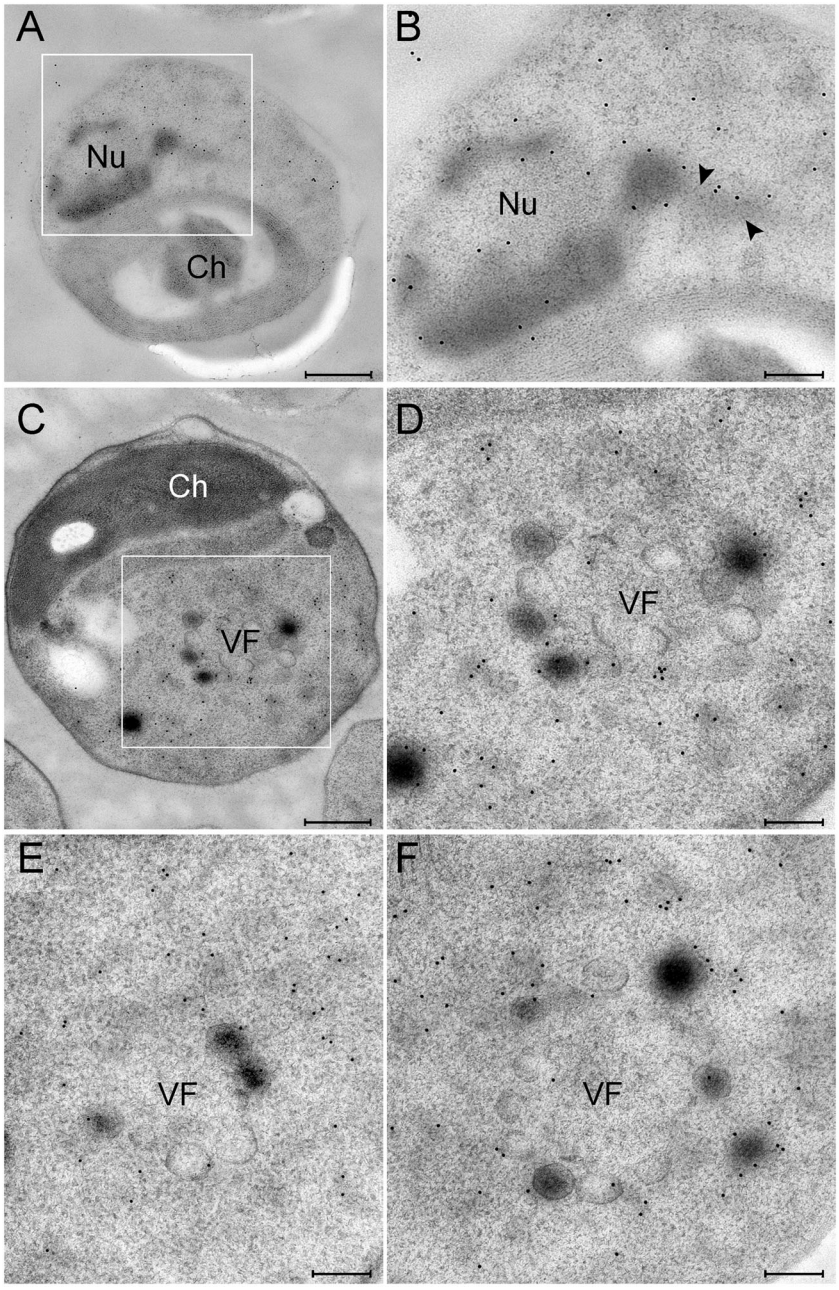

Fig. 5. Localization of viral DNA in PBCV-1 infected *C. variabilis* cells. 2 h PI infected cells were cryo-immobilized and sections were immuno-labelled with anti-DNA antibodies.
A, **C**. Low magnification views of cells exhibiting DNA egress from the nucleus and its accumulation around VFs.
B. High magnification view of the inset in A. Note the density extending from the nucleus towards the cytoplasm (black arrowheads) that is extensively labelled with anti-DNA antibodies. **D**. High magnification view of the inset in C, revealing DNA localization around VFs.
E, **F**. Anti-DNA immuno-labelled cryo-immobilized sections of two additional PBCV-1 infected cells exhibiting DNA spreading around VFs and throughout the host cytoplasm. Scale bars: A, C: 500 nm; B, D–F: 200 nm.

chlorella cells did not reveal any membrane reorganization similar to that detected in PBCV-1 infected cells (Fig. S5; Movie S7). Notably, these observations could only have been obtained with imaging techniques that provide 3D data of entire cells, underscoring the unique advantages of FIB-SEM to study viral infection cycles (Bushby *et al*., 2011; Risco *et al*., 2014).

Discussion

Here, we report key events in the replication cycle of the large DNA chlorovirus PBCV-1 from the Phycodnaviridae family. Our data are consistent with the conjecture that initial DNA replication occurs in host nuclei (Meints *et al*., 1986; Van Etten, 2003; Yamada *et al*., 2006), as is the case for another member of the NCLDV clade, the African Swine Fever virus (ASFV) (Garcia-Beato *et al*., 1992). A nuclear phase of PBCV-1 infection is implied by the lack of a virus-encoded RNA polymerase, as well as by the drastic deformation of the host nuclei shortly following infection. A similar change in nuclear morphology also occurs during infection by the giant *Pandoraviruses* (Philippe *et al*., 2013). Along with bioinformatics analyses, these observations support the conjecture that *Pando-*

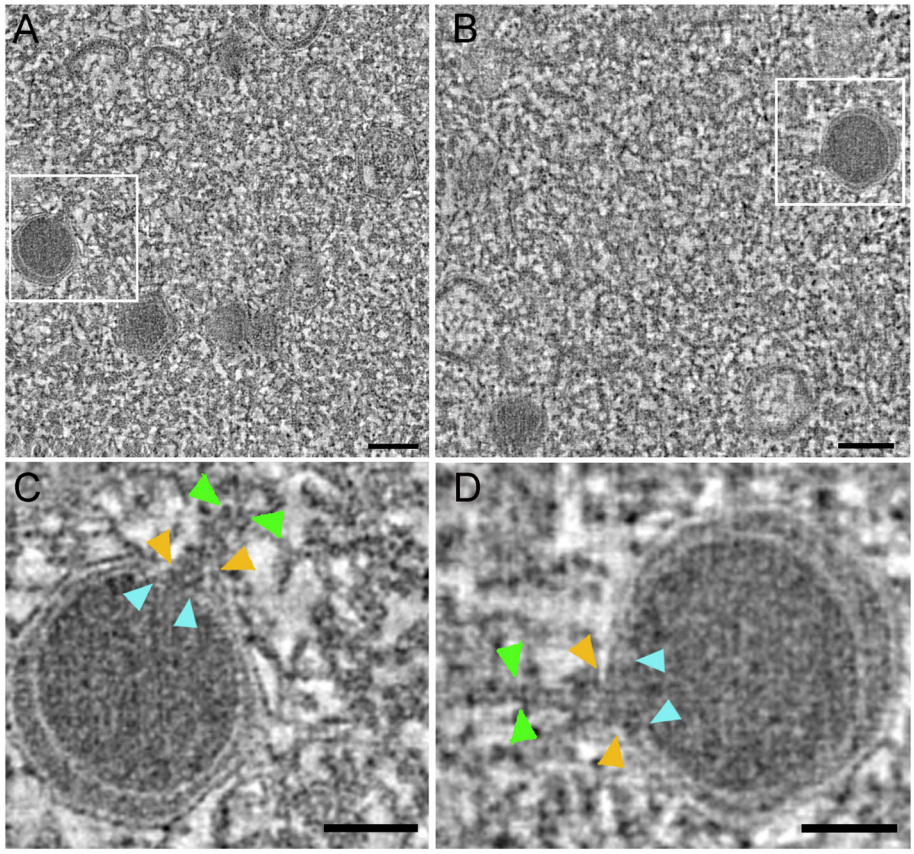

Fig. 6. PBCV-1 genome packaging.
A, **B**. Two slices derived from two different STEM tomography analyses, showing viruses in the process of DNA packaging.
C, **D**. High magnification of the insets indicated in A and B respectively. The aperture located at one of the virus icosahedral vertices is clearly visible. Yellow and light blue arrowheads point to the discontinuity of the capsid and internal membrane layers of the virus respectively. Green arrowheads indicate genomes in the process of encapsidation. Scale bars; A, B: 100 nm; C, D: 50 nm.

raviruses are evolutionarily related to the Phycodnaviruses (Yutin and Koonin, 2013).

The assumption that PBCV-1 replication begins in host nuclei is further supported by a massive DNA egress from the nuclei at later PI time points, which was also demonstrated for ASFV (Garcia-Beato *et al*., 1992). Moreover, the enhanced heterochromicity revealed in infected cells may indicate that PBCV-1 replication occurs at specific regions at the periphery of the host nuclei, as was shown for dsDNA gammaherpes viruses (Peng *et al*., 2010). In contrast, Vaccinia (Tolonen *et al*., 2001; Katsafanas and Moss, 2007; Chichon *et al*., 2009; Suárez *et al*., 2013) and Mimivirus (Zauberman *et al*., 2008; Mutsafi *et al*., 2010; Kuznetsov *et al*., 2013; Mutsafi *et al*., 2013) replicate exclusively in the host cytoplasm. As such, no structural alterations of host nuclei are detected during the infection of these viruses.

The results reported here reveal another significant difference in the infection process among dsDNA viruses belonging to the NCLDV clade. Specifically, *Mimivirus* replication occurs in a distinct location of the host cytoplasm in which viral genomes occupy a central site within the factory, which is surrounded by membrane structures and capsids (Mutsafi *et al*., 2013, 2014). In contrast, our fluorescence and immuno-labelling studies indicate that newly-replicated viral genomes, which correspond to the outer part of the PBCV-1 cytoplasmic factory, are spread throughout the host cytoplasm. Notably, it remains unclear if additional PBCV-1 DNA replication occurs in the cytoplasm or if it occurs exclusively in the nucleus. In light of the fact that bacteriophage infection turns the entire bacterial cell into a viral factory (Forterre, 2010), these findings provide a new angle to the notion that PBCV-1 replication proceeds through a bacteriophage-like infection process (Van Etten, 2003; Wulfmeyer *et al*., 2012).

Previous studies indicated an unusual mode of biogenesis of a single internal membrane bilayer in Vaccinia, *Mimivirus* and the ASFV (Chlanda *et al*., 2009; Krijnse-Locker *et al*., 2013; Mutsafi *et al*., 2013; 2014; Suárez *et al*., 2015; Szajner *et al*., 2005). In these viruses, internal membrane bilayers are generated from host ER cisternae that are recruited to the VFs and subsequently ruptured to form open single bilayer membrane sheets. These single bilayers interact with capsid proteins (Vaccinia D13, Mimivirus L425 and

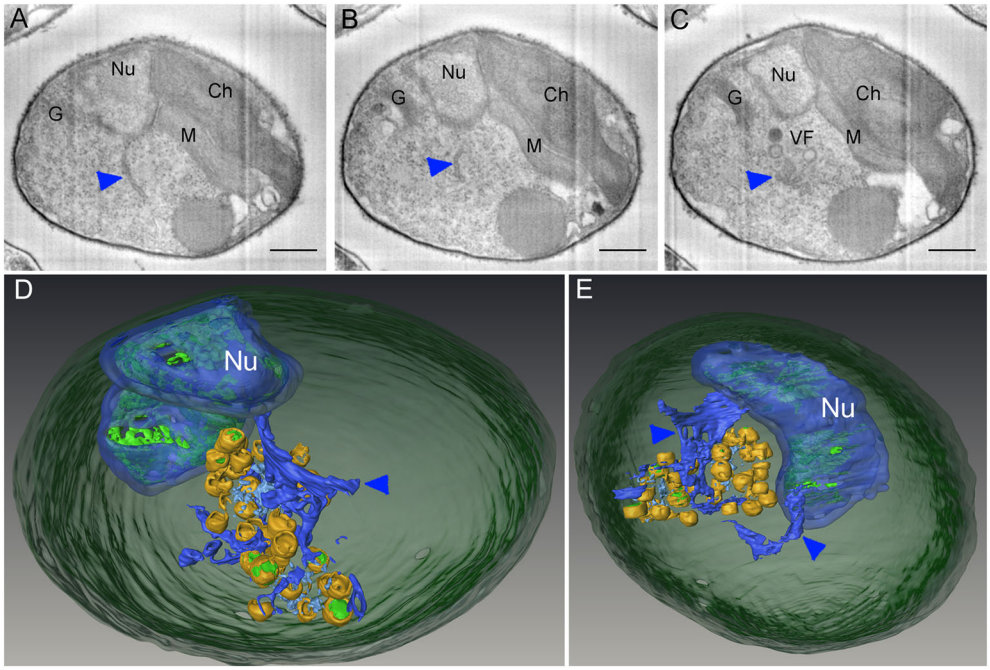

Fig. 7. 3D imaging by FIB-SEM of PBCV-1 infected cells.
A–C (Supported in Fig. S4 and S5 and Movies S5–S7). Three slices from an entire, 3 h PI *C. variabilis* cell (A, top; B, centre; C, bottom), showing cisternae budding from the outer nuclear membrane (A, B, blue arrowheads) and their disassembly into smaller membrane structures (C) that subsequently rupture into open single bilayers at the VF core.
D, **E**. 3D surface-rendering of the entire cell analysed by FIB-SEM showing two views of PBCV-1 factory. Capsids at various maturation stages are depicted in yellow. Host membrane structures including nucleus outer membrane and two distinct cisternae budding from the nucleus are depicted in blue (blue arrowheads). Host and viral DNA and cell wall are indicated in light and dark green respectively. Scale bars: 500 nm.

ASFV p72 proteins) to generate crescents and eventually pre-capsids. Our 3D STEM tomography studies of PBCV-1 infected *C. variabilis* cells reveal that host cisternae also act as precursors of PBCV-1 internal membranes.

Specifically, we suggest that these cisternae are ER membranes that are derived from outer nuclear membranes and studded with ribosomes that are removed as these structures reach PBCV-1 factories. Subsequently, cisternae are ruptured into a dense network of open, single bilayer membrane sheets that accumulate in the centre of the PBCV-1 factories. These open sheets interact with a capsid protein to form pre-capsids, as was shown to be the case for Vaccinia (Chlanda *et al.*, 2009), *Mimivirus* (Krijnse-Locker *et al.*, 2013; Mutsafi *et al.*, 2013) and ASFV (Suárez *et al.*, 2015). Therefore, a general mechanism for the biogenesis of single internal membrane bilayers in viruses, as well as a role for these sheets as templates for crescents formation and capsid assembly, may exist. Notably, the well-ordered rosette-like arrangement of these crescents and of pre-capsids implies that after being ruptured, membrane sheets maintain a structural continuity, presumably due to a constraint diffusion of large macromolecular assemblies within the highly crowded intracellular milieu (Minsky, 2003). It should be noted however that, as is the case for *Mimivirus* (Mutsafi *et al.*, 2013) and ASFV (Suárez *et al.*, 2015), such a structural continuity was not detected by diverse imaging studies. This issue, as well as the proteins responsible for membrane rapture and those promoting stabilization of membrane ends in PBCV-1, *Mimivirus* and ASFV remain to be elucidated.

The observations reported here are summarized in a model for the generation and structure of PBCV-1 cytoplasmic factories (Fig. 8A). The model depicts the main features of PBCV-1 infection, including structural deformation of host nuclei, generation of nuclei-derived cisternae that act as precursors for single bilayer viral membranes, egress of viral genomes from host nuclei that eventually pervade the entire host cell, followed by capsid assembly, virion formation and genome packaging, apparently proceeding through a large portal, as was shown to be the case for the *Mimivirus* (Zauberman *et al.*, 2008). The PBCV-1 model is juxtaposed with a model of the *Mimivirus* factory (Fig. 8B) (Mutsafi *et al.*, 2013).

Significant differences in the structure and generation pathways of PBCV-1, *Mimivirus* and Vaccinia factories notwithstanding, fundamental similarities are evident. A salient similarity is the mechanism of single sheet membrane bilayer generation through rupture of host cisternae. All factories reveal an ordered organization that enables continuous generation of virus progeny,

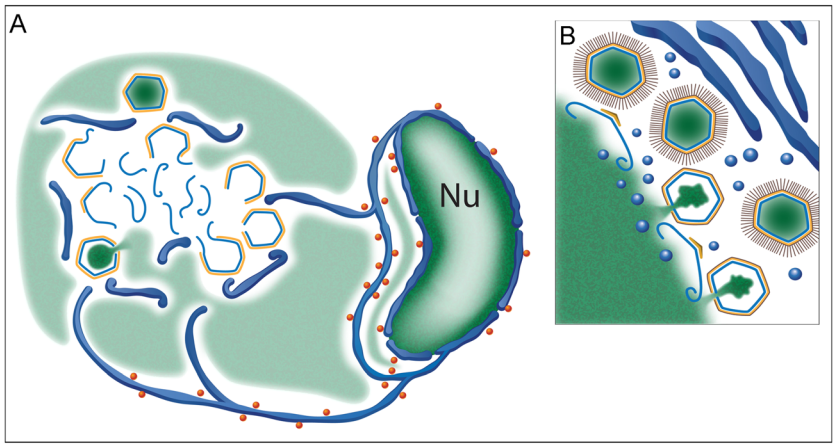

Fig. 8. Models of the generation and structure of PBCV-1 and *Mimivirus* VFs. The observations reported here are summarized in a model of the generation and structure of PBCV-1 cytoplasmic factories (**A**). The model depicts the main features of PBCV-1 assembly into infectious particles, including infection-related deformation of host nuclei (Nu), generation of nuclei-derived cisternae, decorated with ribosomes (red spheres), which act as precursors for single bilayer viral membranes (dark and light blue respectively). The model further reveals the egress of viral genomes from host nuclei that eventually pervade the entire host cell (green) and the formation of cytoplasmic factories. This model is juxtaposed with a model of the *Mimivirus* factory (**B**) (Mutsafi *et al.*, 2013). Differences between the two factories, as well as fundamental similarities, are discussed in the text.

thus acting as highly efficient 'production lines' (Mutsafi *et al.*, 2014). Figure 6 reveals the generation of large portals that enable effective genome encapsidation, reminiscent of those generated by *Mimivirus* virions (Zauberman *et al.*, 2008), and Fig. S6 depicts deconvoluted images of fluorescently-stained uninfected *C. variabilis* cells (A–C), as well as *C. variabilis* cells at progressive PBCV-1 infection stages (D–L), supporting the model shown in Fig. 8A.

The efficiency of VFs is particularly evident during PBCV-1 infection cycle, where apparently mature virions are detected as early as 2 h PI. The implications of the ordered spatial organization of VFs, as well as of eukaryotic nuclei and bacteria, were highlighted by a recent study, which indicated that component clustering results in dramatic acceleration of metabolic transactions (Castellana *et al.*, 2014). The increasing interest in the generation, structure and division of functions of cytoplasmic factories formed by large DNA viruses stems from the notion that these factories may not only provide new insights into the generation of eukaryotic nuclei (Schramm and Krijnse-Locker, 2005; Bell, 2006) but also contribute novel perspectives to our understanding of why highly-ordered architectures represent a recurrent motif in cellular biology.

Experimental procedures

Sample preparation

Chlorella variabilis cultures were cultivated on MBBM medium under continuous illumination and shaking at 25° C (Van Etten *et al.*, 1983) and infected with PBCV-1 at an MOI of 25 at mid-log. For electron microscopy studies infected cells were chemically fixed or high-pressure frozen. The chemical fixation protocol is a modified version of the protocol reported in Terasaki *et al.* (2013). Cells were chemically fixed using 2% (v/v) glutaraldehyde for 2 h at room temperature (RT). After fixation cell pellets were embedded in 3.4% agar (Difco), trimmed and stained with a solution of 1% (v/v) OsO_4 in 0.1M cacodylate buffer at RT. Samples were then stained with 2% (w/v) uranyl acetate (UA) in double distilled water.

Freeze substitution was conducted with freeze substitution machine (Leica EM AFS, Austria) in dry acetone containing 2% glutaraldehyde and 0.1% tannic acid. Samples were gradually warmed to RT and then incubated in 1% UA and 1% OsO_4 for 1 h, infiltrated with increasing Epon concentrations over 7 days. Thin sections (70–100 nm), obtained with an Ultracut UCT microtome (Leica) were post-stained with 2% UA and Reynold's lead citrate. Images were obtained using FEI Spirit TEM operating at 120 kV and recorded on a CCD camera (Eindhoven, the Netherlands) or high-speed Erlangshen camera (Gatan).

Scanning transmission electron microscopy tomography (Aoyama et al., 2008)

Sections of ~250 nm were transferred to 150-mesh copper grids supported by carbon-coated (Edwards) Formvar film, and decorated with 12 nm gold beads on both sides. Tilt series were acquired with FEI Tecnai G2 F20 TEM operated at 200 kV. Automatic sample tilting, focusing and image-shift correction were performed with Xplore3D software (FEI). Double tilt series were acquired at 1.5^0 increments at an angular range of -65^0 to $+65^0$, with Gatan bright-field detector in the nanoprobe STEM mode. 3D reconstructions were computed from tilt series using a weighted back-projection algorithm (Mastronarde, 1997). Tomograms were post processed either with a median or a smoothing filter using IMOD (Kremer *et al.*, 1996). 16 STEM tomograms of 2–3 h PI *C. variabilis* cells and 5 tomograms of 1.5 h PI cells (that do not yet contain viral

factories) were collected and analysed. Volume segmentation, visualization and movies were generated using the Avizo 6.3 image-processing package (FEI visualization sciences group).

Immuno-electron microscopy

Samples were high-pressure frozen and freeze-substituted in dry acetone containing 0.2% UA and 0.1% glutaraldehyde. Samples were then slowly warmed to −20°C, infiltrated with increasing concentrations of LR-Gold, UV-polymerized at −20°C, sectioned and deposited on formvar coated nickel 200 mesh grids. Grids were treated with 0.5–1% blocking solution for 20 min and then incubated with anti-DNA antibody (clone HYB331-01, Abcam). Grids were rinsed with 0.1% glycine in PBS and incubated with 10 nm gold conjugated goat anti-mouse (EMS). Grids were washed with PBSX1 and DDW. Grids were either post-stained with 2% UA and Reynold's lead citrate or not. Samples were visualized using an FEI Tecnai T-12 (FEI Company, Eindhoven, the Netherlands).

Whole-cell focused ion beam-scanning electron microscopy 'slice and view' studies (Bushby et al., 2011)

Epon blocks containing chemically fixed *C. variabilis*-infected cells were trimmed to pyramidal shape. Pyramids were smoothed and mounted on a SEM stub, over which a thin (5–6 nm) carbon layer was deposited (Edwards). Images were acquired using Helios 600 Dual Beam microscope (FEI) equipped with a gallium ion source for focused ion beam milling, with a field emission gun scanning electron microscope and an in-lens secondary electron detector. Sequential surface view imaging was conducted with the View G2 (FEI) programme. Secondary electrons (SE) scanning electron microscope (SEM) images were acquired at 0.34 nA at 2 kV. Milling of serial slices was carried out with an ion beam current of 0.46 nA at 30 kV with 10 nm increments. Images were stacked and aligned using the StackReg plugin programme. Volume segmentation, visualization and movies were generated with the Avizo 6.3 image processing package (FEI visualization sciences group). FIB-SEM experiments were conducted on eight 3 h PI *C. variabilis* cells and on 10 non-infected control cells.

Fluorescence studies

Paramecium bursaria chlorella virus 1 infected *C. variabilis* cells were stained with membrane ($DiOC_6$) and DNA (SYTO82) probes (Molecular probes). Cells were imaged in a Deltavision (Applied Precision) fluorescence microscope. Images were de-convoluted with the conservative SoftWorx package using high noise filtering and 10 iterations. Pearson analyses were conducted as reported (Adler *et al.*, 2008).

Acknowledgements

This research was supported by the Israel Science Foundation (ISF), the German Minerva Foundation and the Israeli Excellence Center (I-CORE) for Integrated Structural and Cell-Biology Studies.

References

Adler, J., Pagakis, S.N., and Parmryd, I. (2008) Rep licate-based noise corrected correlation for accurate measurements of colocalization. *J Microsc* **230**: 121–133.

Agarkova, I.V., Dunigan, D.D., and Van Etten, J.J. (2006) Virion-associated restriction endonucleases of chloroviruses. *J Virol* **80**: 8114–8123.

Ahlquist, P. (2006) Parallels among positive-strand RNA viruses, reverse-transcribing viruses and double-stranded RNA viruses. *Nat Rev Microbiol* **4**: 371–382.

Aoyama, K., Takagi, T., Hirase, A., and Miyazawa, A. (2008) STEM tomography for thick biological specimens. *Ultramicroscopy* **109**: 70–80.

Bell, P.J.L. (2006) Sex and the eukaryotic cell cycle is consistent with a viral ancestry for the eukaryotic nucleus. *J Theoret Biol* **243**: 54–63.

Blanc, G., Mozar, M., Agarkova, I.V., Gurnon, J.R., Yanai-Balser, G., Rowe, J.M., *et al.* (2014) Deep RNA sequencing reveals hidden features and dynamics of early gene transcription in *Paramecium bursaria* chlorella virus 1. *PLoS One* **9**: e90989.

Bowman, G.R., Lyuksyutova, A.I., and Shapiro, L. (2011) Bacterial polarity. *Curr Opin Cell Biol* **23**: 71–77.

Bushby, A.J., P'ng, K.M.Y., Young, R.D., Pinali, C., Knupp, C., and Quantock, A.J. (2011) Imaging three-dimensional tissue architectures by focused ion beam scanning electron microscopy. *Nat Protocols* **6**: 845–858.

Castellana, M., Wilson, M.Z., Xu, Y., Joshi, P., Cristea, I.M., Rabinowitz, J.D., Gitai, Z., and Wingreen, N.S. (2014) Enzyme clustering accelerates processing of intermediates through metabolic channeling. *Nature Biotechnol* **32**: 1011–1018.

Chichon, F.J., Rodriguez, M.J., Risco, C., Fraile-Ramos, A., Fernandez, J.J., Esteban, M., and Carrascosa, J.L. (2009) Membrane remodelling during vaccinia virus morphogenesis. *Biol Cell* **101**: 401–414.

Chlanda, P., Carbajal, M.A., Cyrklaff, M., Griffiths, G., and Krijnse-Locker, J. (2009) Membrane rupture generates single open membrane sheets during Vaccinia virus assembly. *Cell Host Microbe* **6**: 81–90.

Claverie, J.M., and Abergel, C. (2010) *Mimivirus*: the emerging paradox of quasi-autonomous viruses. *Trends Genet* **26**: 431–437.

Claverie, J.M., Abergel, C., and Ogata, H. (2009) *Mimivirus*. In *Lesser Known Large dsDNA Viruses*, Van Etten, J.L. (ed.) Berlin: Springer-Verlag, pp. 89–121.

Condit, R.C. (2007) Vaccinia, Inc. Probing the functional substructure of poxviral replication factories. *Cell Host Microbe* **2**: 205–207.

de Castro, I.F., Volonte, L., and Risco, C. (2013) Virus factories: biogenesis and structural design. *Cell Microbiol* **15**: 24–34.

den Boon, J.A., Diaz, A., and Ahlquist, P. (2010) Cytoplasmic viral replication complexes. *Cell Host Microbe* **8**: 77–85.

den Boon, J.A., and Ahlquist, P. (2010) Organelle-like membrane compartmentalization of positive-strand RNA virus replication factories. *Annu Rev Microbiol* **64**, 241–256.

Earl, L.A., Lifson, J.D., and Subramaniam, S. (2013) Catching HIV 'in the act' with 3D electron microscopy. *Trends Microbiol* **21**: 397–404.

Edelman, L.B., and Fraser, P. (2012) Transcription factories: genetic programming in three dimensions. *Curr Opin Genet Dev* **22**: 110–114.

Fontana, J., Tzeng, W.P., Calderita, G., Fraile-Ramos, A., Frey, T.K., and Risco, C. (2007) Novel replication complex architecture in rubella replicon-transfected cells. *Cell Microbiol* **9**: 875–890.

Forterre, P. (2010) Defining life: the virus viewpoint. *Orig Life Evol Biosph* **40**: 151–160.

Garcia-Beato, R., Salas, M.L., Vinuela, E., and Salas, J. (1992) Role of the host-cell nucleus in the replication of African Swine Fever Virus DNA. *Virology* **188**: 637–649.

Gitai, Z. (2005) The new bacterial cell biology: moving parts and subcellular architecture. *Cell* **120**: 577–586.

Hsu, N.-Y., Ilnytska, O., Belov, G., Santiana, M., Chen, Y.-H., Takvorian, P.M., et al. (2010) Viral reorganization of the secretory pathway generates distinct organelles for RNA replication. *Cell* **141**: 799–811.

Husain, M., Weisberg, A.S., and Moss, B. (2006) Existence of an operative pathway from the endoplasmic reticulum to the immature poxvirus membrane. *Proc Natl Acad Sci U S A* **103**: 19506–19511.

Iyer, L.M., Aravind, L., and Koonin, E.V. (2001) Common origin of four diverse families of large eukaryotic DNA viruses. *J Virol* **75**: 11720–11734.

Katsafanas, G.C., and Moss, B. (2007) Colocalization of transcription and translation within cytoplasmic poxvirus factories coordinates viral expression and subjugates host functions. *Cell Host Microbe* **2**: 221–228.

Kopek, B.G., Perkins, G., Miller, D.J., Ellisman, M.H., and Ahlquist, P. (2007) Three-dimensional analysis of a viral RNA replication complex reveals a virus-induced mini-organelle. *Plos Biol* **5**: 2022–2034.

Kremer, J.R., Mastronarde, D.N., and McIntosh, J.R. (1996) Computer visualization of three-dimensional image data using IMOD. *J Struct Biol* **116**: 71–76.

Krijnse-Locker, J., Chlanda, P., Sachsenheimer, T., and Bruegger, B. (2013) Poxvirus membrane biogenesis: rupture not disruption. *Cell Microbiol* **15**: 190–199.

Kuznetsov, Y.G., Klose, T., Rossmann, M., and McPherson, A. (2013) Morphogenesis of *Mimivirus* and its viral factories: an atomic force microscopy study of infected cells. *J Virol* **87**: 11200–11213.

Laliberte, J.P., and Moss, B. (2010) Lipid membranes in Poxvirus replication. *Viruses* **2**: 972–986.

Llopis, P.M., Jackson, A.F., Sliusarenko, O., Surovtsev, I., Heinritz, J., Emonet, T., and Jacobs-Wagner, C. (2010) Spatial organization of the flow of genetic information in bacteria. *Nature* **466**: 77–81.

Mallardo, M., Leithe, E., Schleich, S., Roos, N., Doglio, L., and Krijnse-Locker, J. (2002) Relationship between Vaccinia virus intracellular cores, early mRNAs, and DNA replication sites. *J Virol* **76**: 5167–5183.

Mallardo, M., Schleich, S., and Krijnse-Locker, J. (2001) Microtubule-dependent organization of Vaccinia virus core-derived early mRNAs into distinct cytoplasmic structures. *Mol Biol Cell* **12**: 3875–3891.

Maruri-Avidal, L., Weisberg, A.S., Bisht, H., and Moss, B. (2013) Analysis of viral membranes formed in cells infected by a Vaccinia virus L2-deletion mutant suggests their origin from the endoplasmic reticulum. *J Virol* **87**: 1861–1871.

Mastronarde, D.N. (1997) Dual-axis tomography: an approach with alignment methods that preserve resolution. *J Struct Biol* **120**: 343–352.

Meaburn, K.J., and Misteli, T. (2007) Chromosome territories. *Nature* **445**, 379–381.

Meints, R.H., Lee, K., and Van Etten, J.L. (1986) Assembly site of the virus PBCV-1 in a Chlorella-like green-alga: ultrastructural studies. *Virology* **154**: 240–245.

Miller, S., and Krijnse-Locker, J. (2008) Modification of intracellular membrane structures for virus replication. *Nat Rev Microbiol* **6**: 363–374.

Minsky, A. (2003) Structural aspects of DNA repair: the role of restricted diffusion. *Mol Microbiol* **50**: 367–376.

Misteli, T. (2004) Spatial positioning: a new dimension in genome function. *Cell* **119**: 153–156.

Misteli, T. (2007) Beyond the sequence: cellular organization of genome function. *Cell* **128**: 787–800.

Moss, B. (2015). Poxvirus membrane biogenesis. *Virology* **479/480**: 619–626.

Mutsafi, Y., Fridmann-Sirkis, Y., Milrot, E., Hevroni, L., and Minsky, A. (2014) Infection cycles of large DNA viruses: emerging themes and underlying questions. *Virology* **466**: 3–14.

Mutsafi, Y., Shimoni, E., Shimon, A., and Minsky, A. (2013) Membrane assembly during the infection cycle of the giant *Mimivirus*. *Plos Pathogens* **9**: e1003367.

Mutsafi, Y., Zauberman, N., Sabanay, I., and Minsky, A. (2010) Vaccinia-like cytoplasmic replication of the giant *Mimivirus*. *Proc Natl Acad Sci U S A* **107**: 5978–5982.

Netherton, C., and Wileman, T. (2011) Virus factories, double membrane vesicles and viroplasm generated in animal cells. *Curr Opin Virol* **1**: 381–387.

Nevo-Dinur, K., Nussbaum-Shochat, A., Ben-Yehuda, S., and Amster-Choder, O. (2011) Translation-independent localization of mRNA in *E. coli*. *Science* **331**: 1081–1084.

Novoa, R.R., Calderita, G., Arranz, R., Fontana, J., Granzow, H., and Risco, C. (2005) Virus factories: associations of cell organelles for viral replication and morphogenesis. *Biol Cell* **97**: 147–172.

Peng, L., Ryazantsev, S., Sun, R., and Zhou, Z.H. (2010) Three-dimensional visualization of Gammaherpesvirus life cycle in host cells by electron tomography. *Structure* **18**: 47–58.

Philippe, N., Legendre, M., Doutre, G., Coute, Y., Poirot, O., Lescot, M., Arslan, D., Seltzer, V., Bertaux, L., Bruley, C., et al. (2013) Pandoraviruses: amoeba viruses with genomes up to 2.5 Mb reaching that of parasitic eukaryotes. *Science* **341**: 281–286.

Raoult, D., Audic, S., Robert, C., Abergel, C., Renesto, P., Ogata, H., La Scola, B., Suzan, M., and Claverie, J.M.

(2004). The 1.2-megabase genome sequence of *Mimivirus*. *Science* **306**: 1344–1350.
Risco, C., de Castro, I.F., Sanz-Sanchez, L., Narayan, K., Grandinetti, G., and Subramaniam, S. (2014) Three-dimensional imaging of viral infections. *Annu Rev Virol* **1**: 453–473.
Risco, C., Rodriguez, J.R., Lopez-Iglesias, C., Carrascosa, J. L., Esteban, M., and Rodriguez, D. (2002) Endoplasmic reticulum-Golgi intermediate compartment membranes and vimentin filaments participate in Vaccinia virus assembly. *J Virol* **76**: 1839–1855.
Schramm, B., and Krijnse-Locker, J. (2005) Cytoplasmic organization of POXvirus DNA replication. *Traffic* **6**: 839–846.
Shapiro, L., McAdams, H.H., and Losick, R. (2009) Why and how bacteria localize proteins. *Science* **326**: 1225–1228.
Suárez, C., Welsch, S., Chlanda, P., Hagen, W., Hoppe, S., Kolovou, A., Pagnier, I., Raoult, D., and Krijnse-Locker, J. (2013) Open membranes are the precursors for assembly of large DNA viruses. *Cell Microbiol* **15**: 1883–1895.
Suárez, C., Andres, G., Kolovou, A., Hoppe, S., Salas, M.L., Walther, P., and Krijnse-Locker, J. (2015) African Swine Fever Virus assembles a single membrane derived from rupture of the endoplasmic reticulum. *Cell Microbiol doi*: 10.1111/cmi.12468.
Szajner, P., Weisberg, A.S., Lebowitz, J., Heuser, J., and Moss, B. (2005). External scaffold of spherical immature poxvirus particles is made of protein trimers, forming a honeycomb lattice. *J Cell Biol* **170**: 971–981.
Takizawa, T., Meaburn, K.J., and Misteli, T. (2008) The meaning of gene positioning. *Cell* **135**: 9–13.
Terasaki, M., and Reese, T.S. (1992) Characterization of endoplasmic-reticulum by colocalization of bip and dicarbocyanine dyes. *J Cell Science* **101**: 315–322.
Terasaki, M., Shemesh, T., Kasthuri, N., Klemm, R.W., Schalek, R., Hayworth, K.J., Hand, A.R., Yankova, M., Huber, G., et al. (2013) Stacked endoplasmic reticulum sheets are connected by helicoidal membrane motifs. *Cell* **154**: 285–296.
Thanbichler, M., and Shapiro, L. (2008) Getting organized - how bacterial cells move proteins and DNA. *Nat Rev Microbiol* **6**: 28–40.
Tolonen, N., Doglio, L., Schleich, S., and Krijnse-Locker, J. (2001) Vaccinia virus DNA replication occurs in endoplasmic reticulum-enclosed cytoplasmic mini-nuclei. *Mol Biol Cell* **12**: 2031–2046.
Van Etten, J.L., Burbank, D.E., and Meints, R.H. (1983) Virus infection of culturable chlorella-like algae and development of plaque assay. *Science* **219**: 994–996.
Van Etten, J.L. (2003) Unusual life style of giant chlorella viruses. *Annu Rev Genet* **37**: 153–195.
Van Etten, J.L., Burbank, D.E., Joshi, J., and Meints, R.H. (1984) DNA-synthesis in a chlorella-like alga following infection with the virus PBCV-1. *Virology* **134**: 443–449.
Van Etten, J.L., and Dunigan, D.D. (2012) Chloroviruses: not your everyday plant virus. *Trends Plant Sci* **17**: 1–8.
Van Etten, J.L., Lane, L.C., and Dunigan, D.D. (2010) DNA viruses: the really big ones (giruses). *Annu Rev Microbiol* **64**: 83–99.
Wileman, T. (2006) Aggresomes and autophagy generate sites for virus replication. *Science* **312**: 875–878.
Wulfmeyer, T., Polzer, C., Hiepler, G., Hamacher, K., Shoeman, R., Dunigan, D.D., Van Etten, J.L., Lolicato, M., Moroni, A., Thiel, G., and Meckel, T. (2012) Structural organization of DNA in chlorella viruses. *Plos One* **7**: e30133.
Yamada, T., Onimatsu, H., and Van Etten, J.L. (2006) Chlorella viruses. *Adv Virus Res* **66**: 293–336.
Yolken, R.H., Jones-Brando, L., Dunigan, D.D., Kannan, G., Dickerson, F., Severance, E., Sabunciyan, S., Talbot, C.C., Prandovszky, E., et al. (2014) Chlorovirus ATCV-1 is part of the human oropharyngeal virome and is associated with changes in cognitive functions in humans and mice. *Proc Natl Acad Sci U S A* **111**: 16106–16111.
Yutin, N., and Koonin, E.V. (2013) *Pandoraviruses* are highly derived phycodnaviruses. *Biol Direct* **8**: Article # 25.
Zauberman, N., Mutsafi, Y., Ben Halevy, D., Shimoni, E., Klein, E., Xiao, C., Sun, S., and Minsky, A. (2008) Distinct DNA exit and packaging portals in the virus *Acanthamoeba polyphaga Mimivirus*. *Plos Biol* **6**: 1104–1114.

Supporting information

Additional Supporting Information may be found in the online version of this article at the publisher's web-site:

Fig. S1. 3D surface rendering views of the tomogram presented in Fig. 3, panels G-H.

Fig. S2. PBCV-1 membrane biogenesis, supporting Fig. 3.

Fig. S3. PBCV-1 Chlorella-infected cells at 4h PI, supporting Fig. 4A-D.

Fig. S4. A 3h PI *C. variabilis* cell infected with PBCV-1 was analyzed with a 'Slice and View' FIB-SEM, corresponding to Fig. 7, Movies S5, S6.

Fig. S5. 3D view of a control, non-infected *C. variabilis* cell analyzed by FIB-SEM, supporting data shown in Movie S7.

Fig. S6. Fluorescent images of non-infected as well as PBCV-1-infected *C. variabilis* cells at various PI stages, supporting the model shown in Figure 8A.

Movie S1. 3D surface rendering of the rosette-like PBCV-1 viral factories.

Movies S2; S3. PBCV-1 factories exhibit a complex membrane network composed of host cisternae and single-bilayers open membrane sheets.

Movie S4. Tomogram and 3D surface-rendering of PBCV-1 VF.

Movies S5; S6. FIB-SEM "Slice and View" movies showing 3h-PI PBCV-1-infected *C. variabilis* cells derived from whole cells.

Movie S7. FIB-SEM "Slice and View" movie showing a control, non infected *C. variabilis* cell.